Opposite Skills of ENGPI and DGPI in Depicting Decadal Variability of Tropical Cyclone Genesis over the Western North Pacific

CHAO WANG,[a,b] YIRAN WANG,[a] BIN WANG,[b,c] LIGUANG WU,[d] HAIKUN ZHAO,[a] AND JIAN CAO[a,b]

[a] *Key Laboratory of Meteorological Disaster of Ministry of Education, Collaborative Innovation Center on Forecast and Evaluation of Meteorological Disasters, Joint International Research Laboratory of Climate and Environment Change, Nanjing University of Information Science and Technology, Nanjing, China*
[b] *Earth System Modeling Center, Nanjing University of Information Science and Technology, Nanjing, China*
[c] *Department of Atmospheric Sciences and International Pacific Research Center, University of Hawai'i at Mānoa, Honolulu, Hawaii*
[d] *Department of Atmospheric and Oceanic Sciences and Institute of Atmospheric Sciences, Fudan University, Shanghai, China*

(Manuscript received 5 April 2023, in final form 15 September 2023, accepted 18 September 2023)

ABSTRACT: The genesis potential index (GPI) has been used widely to estimate the influence of large-scale conditions on tropical cyclone (TC) genesis. Here we find that two GPIs, the Emanuel–Nolan GPI (ENGPI) and the dynamic GPI (DGPI), show opposite skills in quantifying decadal variability of TC genesis in the western North Pacific (WNP). During 1979–2020, ENGPI shows a reverse decadal variation to the WNP TC genesis with a significant negative correlation of −0.61, while DGPI can reasonably reproduce the decadal variation of the WNP TC genesis with a significant correlation of 0.66. The opposite skills of the two indices arise from the opposed effects of dynamic and thermodynamic parameters on TC genesis induced by a WNP anomalous cyclonic circulation that controls the decadal variation of TC genesis. On the one hand, the cyclonic circulation leads to favorable dynamical conditions including ascending motion, cyclonic vorticity, and weakened vertical shear, and thus tends to increase the DGPI. On the other hand, the cyclonic circulation leads to unfavorable thermodynamical conditions (decreased maximum potential intensity and midlevel humidity) that tends to decrease the ENGPI. As a result, the DGPI and ENGPI are reversely evolved and eventually lead to their opposite correlation between TC genesis. The significant positive correlation between DGPI and TC genesis suggests a critical role in the large-scale dynamical control of the decadal variability of the WNP TC genesis.

SIGNIFICANCE STATEMENT: Tropical cyclones (TCs) account for one-third of the deaths and economic losses from weather-, climate-, and water-related disasters. Understanding variations in TC activity from the perspective of large-scale conditions is of great importance to seasonal forecasting and disaster mitigation. Here we find that two genesis potential indexes (GPIs), the Emanuel–Nolan GPI (ENGPI) and dynamic GPI (DGPI), show opposite skill in quantifying decadal variability of TC genesis in the western North Pacific (WNP). The opposite skills of the two indices arise from the opposed effects of dynamic and thermodynamic parameters on TC genesis. The result suggests a critical role of large-scale dynamic control in the decadal variability of TC genesis in the WNP.

KEYWORDS: Tropical cyclones; Decadal variability; Climate variability

1. Introduction

Tropical cyclone (TC) genesis requires constructive large-scale environmental conditions (Gray 1968). Extensive efforts have been dedicated to establishing the quantitative connection between large-scale conditions and TC genesis. Gray (1979) first proposed a genesis potential index (GPI) by constructing a function of dynamical and thermodynamical large-scale environmental parameters that are known to be important to TC formation. Several variants of GPI were subsequently developed to improve the quantitative linkage between TC genesis and large-scale environmental conditions from different perspectives (Emanuel and Nolan 2004; Emanuel 2010; Murakami and Wang 2010; Tippett et al. 2011; Menkes et al. 2011; Holland and Bruyère 2013; Zhang et al. 2016; Wang and Moon 2017; Moon et al. 2018; Wang and Murakami 2020). Among them, the GPI proposed by Emanuel and Nolan (2004; ENGPI) is one of the most popular (Camargo et al. 2007). Meanwhile, the recently proposed dynamic GPI (DGPI; Wang and Murakami 2020) shows some advantages in depicting temporal variations of TC genesis (Wang et al. 2021; Murakami and Wang 2022). These two GPIs were widely used to investigate the influence of large-scale environments on TC genesis on various time scales.

On the intraseasonal time scale, it is found that the ENGPI shows a moderate skill in depicting intraseasonal variations of TC genesis, and the low-level absolute vorticity and the midlevel relative humidity are found to be the two most important factors affecting TC genesis (Camargo et al. 2009; Zhao et al. 2015). Wang and Moon (2017) examined the MJO's modulation of TC genesis and found that the most effective factors controlling intraseasonal TC genesis are dynamic parameters such as 850-hPa relative vorticity and midlevel vertical motion. The results suggest that dynamical control is important for TC genesis on the intraseasonal time scale.

On the interannual time scale, both the ENGPI and DGPI show reasonable skill in reproducing the ENSO's impact on TC genesis (Camargo et al. 2007), with suppressed TC genesis

Corresponding authors: Chao Wang, wangchao@nuist.edu.cn; Bin Wang, wangbin@hawaii.edu

DOI: 10.1175/JCLI-D-23-0201.1

in the North Atlantic and the western part of the western North Pacific but an increase in the eastern and central Pacific (Camargo et al. 2007; Menkes et al. 2011; Wang and Murakami 2020). Wang and Murakami (2020) found that ENGPI has good skill in representing interannual variations of TC genesis frequency in the Atlantic and eastern Pacific but no skill in the WNP ($r = -0.04$). In contrast, DGPI has a significant skill ($r = 0.55$) in depicting year-to-year variation of the WNP TC genesis.

For future projection, while TC-permitting models project a decreased TC genesis number in future warming scenarios (Roberts et al. 2020; Knutson et al. 2020), the ENGPI shows a significant increase in CMIP5 and CMIP6 models (Camargo et al. 2014; Knutson et al. 2020; Emanuel 2021). The disparity may result from the increase in thermodynamic factors such as maximum potential intensity (MPI), which increases with global warming–induced rising sea surface temperature (SST) (Emanuel 1999). Murakami and Wang (2022) found that DGPI projects a moderate decrease or no change, which is more consistent with the changes in TC genesis produced by the TC-permitting model compared to that of ENGPI (Roberts et al. 2020). The moderate decrease in TC genesis indicated by DGPI is found to be primarily linked to the future weakening of the midlevel ascending motion, suggesting the prominence of the dynamic parameters in determining TC genesis in global warming scenarios.

Besides the notable variations of TC genesis on the intraseasonal and interannual time scales, the WNP TC genesis exhibits remarkable decadal variations (Liu and Chan 2013; Wu et al. 2015; Hu et al. 2018; Wang et al. 2022). So far, no one has compared the two indices' performance in representing the interdecadal variability of TC genesis. The objective of this study is to examine the skills of the two GPIs in characterizing the decadal variation of the WNP TC genesis and to investigate the key large-scale parameters controlling it. The results obtained here can fill the knowledge gap in the large-scale influences on decadal variation of TC genesis in the WNP.

The remainder of this paper is organized as follows. Section 2 describes the data and methods. Section 3 exhibits the performances of DGPI and ENGPI in depicting decadal variability of the WNP TC genesis, and section 4 explores the role of dynamic and thermodynamic environmental parameters. A summary and discussion are presented in section 5.

2. Data and method

TC genesis information was derived from the International Best Track Archive for Climate Stewardship version 4 (IBTrACS; Knapp et al. 2010), which contains 6-hourly TC location and intensity records issued by forecast centers worldwide. Here three best track datasets over the WNP, namely the Shanghai Typhoon Institute of Chinese Meteorology Administration (CMA), the Regional Specialized Meteorological Center of Japan Meteorological Agency (JMA), and the Joint Typhoon Warning Center (JTWC), were used to count the TC genesis number. Since the results using three datasets are generally similar, only the results using CMA dataset are presented. TCs are defined as the records whose lifetime maximum intensity of wind speeds is greater than or equal to 17.2 m s^{-1}. The monthly mean SST data were obtained from the National Oceanic and Atmospheric Administration (NOAA) Extended Reconstructed SST version 5 (Huang et al. 2017). Two monthly atmospheric reanalysis datasets from the NCEP-DOE Reanalysis (Kanamitsu et al. 2002) and the Japanese 55-year Reanalysis (JRA-55; Kobayashi et al. 2015) were used to derive the large-scale parameters important for TC genesis.

The ENGPI (Emanuel and Nolan 2004) is defined as follows:

$$\mathrm{ENGPI} = |10^5\eta|^{3/2}\left(\frac{\mathrm{RH}}{50}\right)^3\left(\frac{\mathrm{PI}}{70}\right)^3(1 + 0.1V_{\mathrm{shear}})^{-2},$$

where η is the absolute vorticity (s^{-1}) at 850 hPa, RH is the relative humidity at 600 hPa, PI is the potential intensity (m s^{-1}) (Bister and Emanuel 1998), and V_{shear} represents the vertical wind shear (m s^{-1}) between 850 and 200 hPa.

The DGPI (Wang and Murakami 2020) is defined as follows:

$$\mathrm{DGPI} = (2 + 0.1V_s)^{-1.7}\left(5.5 - \frac{\partial u}{\partial y}10^5\right)^{2.3}(5 - 20\omega)^{3.3} \times (5.5 + |10^5\eta|)^{2.4}e^{-11.8} - 1,$$

where the terms of V_s is the vertical wind shear (m s^{-1}) between 850 and 200 hPa, $\partial u/\partial y$ represents the meridional gradient of zonal wind (s^{-1}) at 500 hPa, ω is the vertical velocity (Pa s^{-1}) at 500 hPa, and η is the absolute vorticity (s^{-1}) at 850 hPa.

The total moisture tendency equation at 600 hPa was used to diagnose the dominant factors causing the moisture anomaly (Yanai et al. 1973). The equation can be written as

$$\frac{\partial q'}{\partial t} = -(\mathbf{V}\cdot\nabla q)' - \left(\omega\frac{\partial q}{\partial p}\right)' - \left(\frac{Q_2}{L}\right)',$$

where q is the specific humidity, $\mathbf{V}$ is the horizontal velocity, ∇ is the horizontal gradient operator, ω is the vertical velocity, Q_2 represents the apparent moisture sink, and L is the latent heat constant. Also, the term $-(\mathbf{V}\cdot\nabla q)'$ denotes anomalous horizontal moisture advection, $-[\omega(\partial q/\partial p)]'$ represents anomalous vertical moisture advection, and $-(Q_2/L)'$ denotes an anomalous moisture source or sink.

We focus on the TC that occurred in the WNP (0°–40°N, 100°E–180°) during 1979–2020. Here we choose 1979 as the starting year because routine geostationary satellite monitoring became available around this year, indicating relatively high reliability of TC best track data. The linear trends were first removed and then a 5-yr running mean was applied to all observational data to extract the decadal variability. Statistical significance of regression and correlation analyses were assessed using the two-tailed Student's t test (Wilks 2006). Because the running mean tends to decrease the degree of freedom, the effective degree of freedom was used to estimate the significance of correlation and regression coefficients between the running mean variables (Davis 1976).

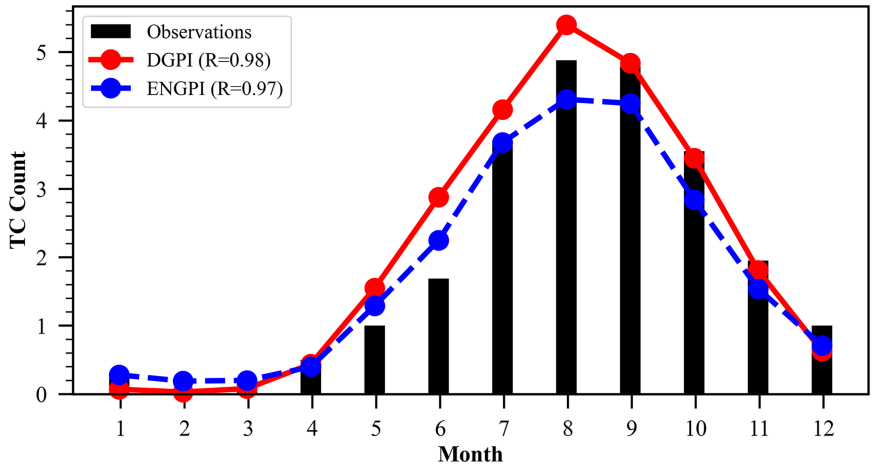

FIG. 1. Annual cycle of TC genesis in the WNP derived from the CMA (black bars), DGPI (red solid line), and ENGPI (blue dashed line) derived from the JRA-55 reanalysis. The correlation coefficients of TC genesis between DGPI and ENGPI are shown at the top left of the panel.

3. Skill of DGPI and ENGPI in depicting the decadal variability of TC genesis

Let us examine climatology first. For the seasonal evolution, TC genesis is relatively inactive in the boreal winter with a minimum in February, gradually turns to active in the summer season peaking in August, and then tends to be quiescent in winter (Fig. 1). The seasonal cycle of TC genesis is generally consistent with the evolution of the WNP summer monsoon (Wang and LinHo 2002), which provides many favorable background large-scale conditions. Since coefficients of DGPI and ENGPI are determined to fit the observed spatial distribution of TC genesis and their magnitudes may not be consistent with observation, here we just focus on their monthly evolution. Generally, both the DGPI and ENGPI can reasonably reproduce the seasonal cycle of TC genesis including the maximum in August and minimum in February, resulting in a significant correlation of 0.98 and 0.97, respectively (Fig. 1). We can find that most TCs occur in July–October (Fig. 1), accounting for about 70% of the total genesis number in a calendar year over the WNP. Therefore, only TC genesis during the main TC season (July–October) is considered in the following. For the spatial distribution, most TC genesis in the WNP during July–October occurs in the region 7.5°–30°N, 110°–170°E with three maximum centers located in the South China Sea and the west and east Philippine Sea, respectively (Fig. 2). The main genesis region is associated with the configuration of four large-scale circulations over the WNP, including the monsoon trough, North Pacific subtropical high, South Asian high, and tropical upper tropospheric trough (Wang and Wu 2016; Wang and Wang 2019, 2021). These circulation systems collectively determine the region of favorable large-scale conditions for TC genesis in the WNP. DGPI can reasonably reproduce the spatial distribution and the location of the maximum zone of TC genesis over the WNP, although the DGPI's maximum center in the South China Sea slightly shifts eastward (Fig. 2a). For the ENGPI, the maximum zone extends from the northern South China Sea and to the sea east of Taiwan, showing a northwestward displacement compared to the observation (Fig. 2b). Accordingly, the spatial correlation of TC genesis between DGPI (0.89) is higher than that of ENGPI (0.84), suggesting the comparable but better skill of DGPI in reproducing spatial distribution of TC genesis over the WNP than that of ENGPI. The results suggest both the DGPI and ENGPI

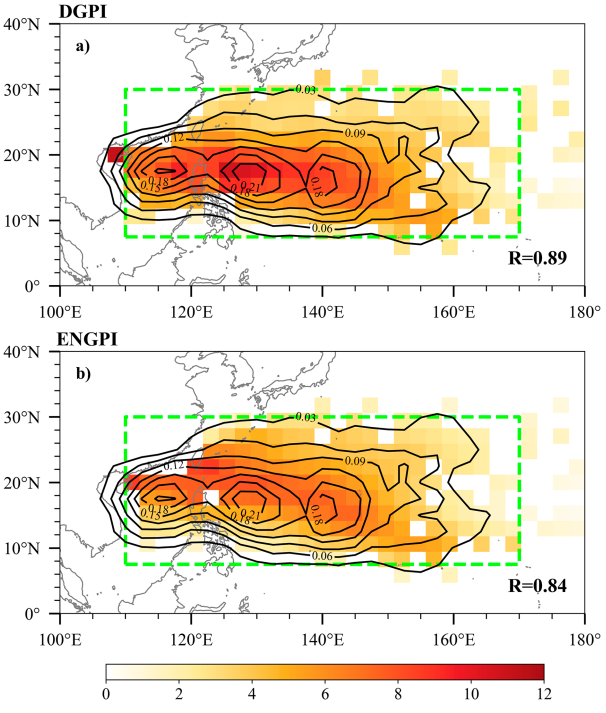

FIG. 2. Climatological mean (a) DGPI and (b) ENGPI (shading) in July–October during 1979–2020 derived from the JRA-55 reanalysis. Contours show the mean genesis frequency in each 2.5° latitude × 2.5° longitude grid box. The green boxes outline the main genesis region (7.5°–30°N, 110°–170°E) over the WNP. The pattern correlation coefficients R of TC genesis frequency with ENGPI and DGPI are shown in the lower right of the panels.

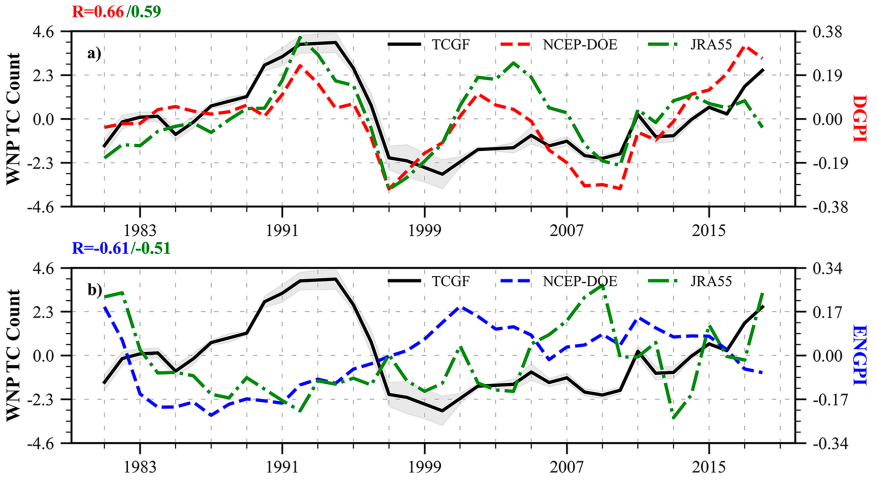

FIG. 3. Time series of 5-yr running mean of TC genesis frequency (black solid line) and (a) DGPI (dashed lines) and (b) ENGPI (dashed lines) over the main genesis region (7.5°–30°N, 110°–170°E) in July–October during 1979–2020 derived from NCEP–DOE and JRA-55 reanalysis. Their correlation coefficients R are shown at the top left of the panels.

show comparable and reasonable skill in depicting the seasonality and spatial distribution of TC genesis in the WNP.

In terms of temporal variation, the skills of DGPI and ENGPI in depicting the decadal variation of TC genesis show a remarkable difference (Fig. 3). TC genesis frequency in the WNP experienced an active epoch from the late 1970s to the late 1990s, followed by an inactive period continuing to the early 2010s, and has returned to being relatively active in recent years (Fig. 3). Generally, the DGPI reasonably reproduces the decadal variation of TC genesis frequency in the WNP (Fig. 3a), with a significant correlation coefficient of 0.66 ($p < 0.05$) tested by the effective degree of freedom. In contrast, the ENGPI shows an almost opposite evolution compared to that in TC genesis (Fig. 3b), which shows low ENGPI before the late 1990s but relatively high ENGPI since the early 2000s. As a result, the ENGPI and TC results are negatively correlated with a significant negative correlation of −0.61 ($p < 0.05$). One concern is that the opposite skill may depend on the reanalysis data, so a state-of-the-art reanalysis, JRA-55, was adopted to further confirm the robustness (Fig. 3). It is found that the opposite correlation of TC genesis between ENGPI and DGPI still exists. Particularly, TC genesis is positively correlated with the DGPI with a correlation of 0.59 ($p < 0.05$), while it is negatively correlated with the ENGPI with a correlation of −0.51 ($p < 0.05$). The consistency of the results derived from two reanalysis datasets confirms the robustness of their opposite skills and lends us confidence to further investigate the root cause. The negative correlation of ENGPI implies that some components of ENGPI are destructive and even counterproductive in depicting the decadal variation of TC genesis in the WNP.

4. Role of dynamic and thermodynamic environmental parameters

Why do the DGPI and ENGPI possess opposed skills in depicting the decadal variation of TC genesis in the WNP? To investigate the major factors resulting in the opposite relationship, we first examined the linear correlation of TC genesis between the four large-scale parameters of DGPI and ENGPI (Figs. 4 and 5). The linear correlation between TC genesis and 500-hPa vertical motion, meridional gradient of 500-hPa zonal wind, vertical wind shear, and 850-hPa absolute vorticity over the main genesis region for the NCEP–DOE (JRA-55) dataset is −0.55 (−0.48), 0.01 (0.19), −0.46 (0.3), and 0.29 (0.28), respectively (Fig. 4a). The high correlations of 500-hPa vertical motion and vertical wind shear indicate their important contribution to significant correlation between DGPI and TC genesis. To quantitatively confirm the contribution of each component, we recalculated the correlation of TC genesis between DGPI by varying each component with the other three components fixed as their climatology (Fig. 4b). It can be found that the midlevel vertical motion term has the foremost contribution, followed by the vertical wind shear term and absolute vorticity term, while the contribution of the meridional gradient of 500-hPa zonal wind term is negligible (Fig. 4b).

For the four large-scale parameters in ENGPI, the correlations of TC genesis between MPI, 600-hPa relative humidity, vertical wind shear, and 850-hPa absolute vorticity over the main genesis region for NCEP–DOE (JRA-55) are −0.51 (−0.69), −0.25 (−0.23), −0.46 (−0.3), and 0.29 (0.28), respectively (Fig. 5a). It is unexpected that MPI and midlevel humidity are negatively correlated with TC genesis, which are supposed to increase with the possibility of TC genesis (Emanuel and Nolan 2004; Camargo et al. 2007). Accordingly, we recalculated the correlation of TC genesis between ENGPI by varying each component with the other three components fixed as their climatology. Although the positive contribution of vertical wind shear term and low-level absolute vorticity term still exists, the negative effect of the MPI term ($R = -0.48$ for NCEP–DOE and $R = -0.67$ for JRA-55) and relative humidity term ($R = -0.46$ for NCEP–DOE and $R = -0.25$ for JRA-55)

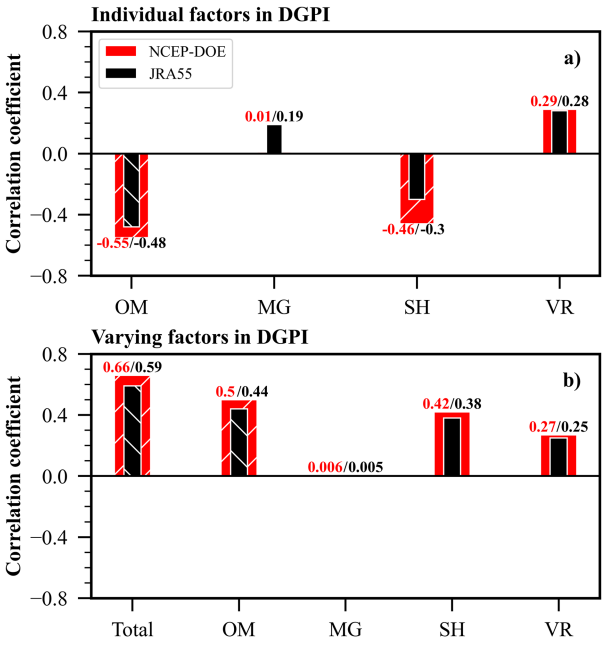

FIG. 4. Correlation coefficients of TC genesis frequency between (a) 500-hPa omega (OM), the meridional gradient of zonal wind (MG), vertical wind shear (SH), and 850-hPa absolute vorticity (VR) over 7.5°–30°N, 110°–170°E in July–October during 1979–2020, and (b) correlation coefficients of TC genesis frequency between DGPI (total), DGPI derived from varying OM, MG, SH, and VR over 7.5°–30°N, 110°–170°E in July–October during 1979–2020, respectively, with the other three variables fixed as climatology. The red and black bars represent correlations between TC genesis and DGPI derived from the NCEP–DOE and JRA-55 reanalysis, respectively. The hatched bars denote the correlations that are significant at the 95% confidence levels. The numbers denote the corresponding correlation coefficients.

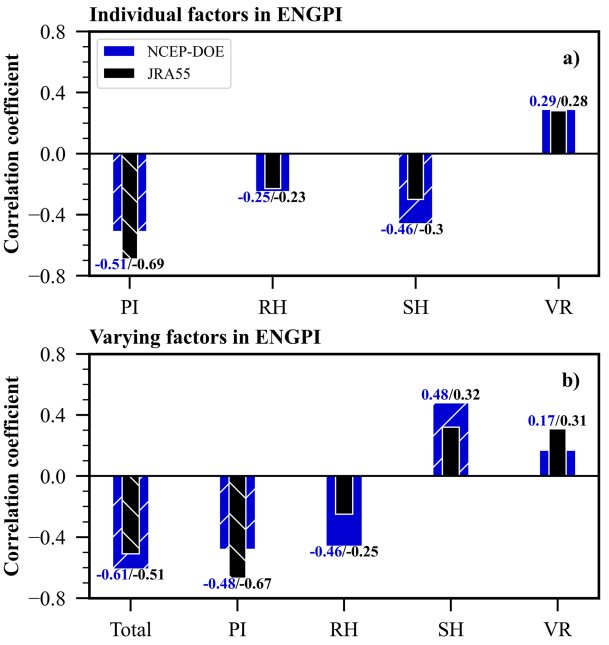

FIG. 5. (a) Correlation coefficients of TC genesis frequency between maximum potential intensity (PI), relative humidity (RH), vertical wind shear (SH), and 850-hPa absolute vorticity (VR) over 7.5°–30°N, 110°–170°E in July–October during 1979–2020. (b) Correlation coefficients of TC genesis frequency between ENGPI (total) and ENGPI derived from varying PI, RH, SH, and VR over 7.5°–30°N, 110°–170°E in July–October during 1979–2020, respectively, with the other three variables fixed as climatology. The blue and black bars represent correlations between TC genesis and ENGPI derived from the NCEP–DOE and JRA-55 reanalysis, respectively. The hatched bars denote the correlations that are significant at the 95% confidence levels. The numbers denote the corresponding correlation coefficients.

overwhelm their positive contributions (Fig. 5a), eventually leading to the significant negative correlation between the ENGPI and TC genesis (Fig. 5b). Thus, we can conclude that the MPI and relative humidity term are the major contributors for the significant negative correlation between ENGPI and TC genesis in the WNP.

MPI and relative humidity reflect a lot of the thermodynamic requirement for TC formation, it is usually supposed that greater MPI and midlevel humidity indicate a more favorable thermodynamic condition and higher possibility for TC genesis, and thus a greater value of ENGPI (Emanuel and Nolan 2004; Camargo et al. 2007). To understand the negative contribution of MPI and relative humidity to TC genesis in the WNP, we examined the regressed large-scale circulation and underlying boundary condition anomalies against the WNP TC genesis (Fig. 6). The 850-hPa winds feature an anomalous cyclonic circulation extended from the subtropical eastern North Pacific to the WNP (Fig. 6a), which provides the anomalous ascending motion, weakened vertical shear, and cyclonic vorticity that are conducive to TC genesis in the WNP (Figs. 4 and 6c). Meanwhile, the westerly to the south flank of the cyclonic circulation tends to decrease the zonal gradient over the tropical Pacific, and then reinforce westerly anomalies through Bjerknes feedback (Bjerknes 1969), eventually resulting in the negative SST anomalies (Fig. 6a). Since the tropopause temperature can be influenced by the SST (Emanuel 1987; Reid and Gage 1981; DeMaria and Kaplan 1994), variations in boundary SST largely control changes in MPI. As a result, the regressed MPI shows a similar pattern to that of SST, with significant negative anomalies in the WNP (Figs. 6a,b). The time series of SST and MPI were further examined to confirm their relationship (Fig. 7).

It can be found that both decadal variations of MPI derived from the two reanalysis datasets are significantly correlated with SST, indicating the key role of SST in the decadal variations of MPI. A remaining issue is why negative relative humidity anomalies occur in the main genesis region with the assistance of anomalous ascending motion. A moisture budget analysis (Yanai et al. 1973; Weng et al. 2022) was conducted to understand the negative humidity anomalies (Fig. 8). Since the diagnostic results from the NCEP–DOE and JRA-55 are similar, here only the results from NCEP–DOE are presented. It can be found that the positive contribution of vertical advection by ascending motion is largely offset by negative contribution of the moisture loss due to the associated condensation, while the horizontal

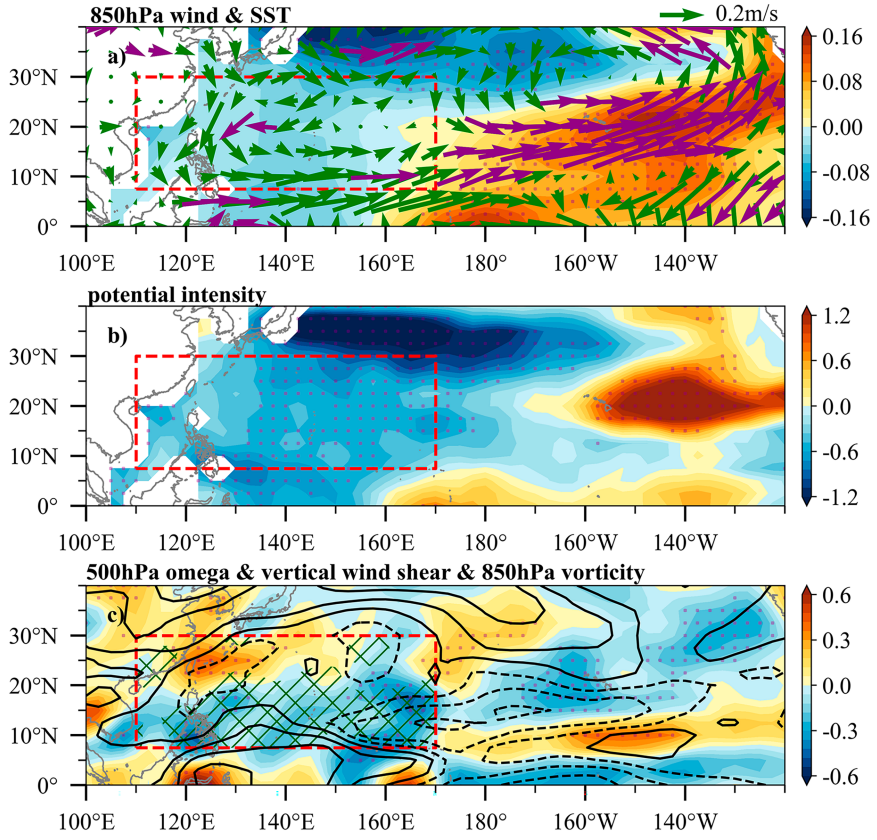

FIG. 6. Regressed (a) SST (shading; °C) and 850-hPa winds (vectors; m s^{-1}); (b) maximum potential intensity (shading; m s^{-1}); and (c) 500-hPa vertical pressure velocity (shading; 10^{-2} Pa s^{-1}), vertical wind shear (contours; m s^{-1}), and absolute vorticity (hash marked region; 10^{-6} s^{-1}) anomalies from NCEP–DOE reanalysis against the time series of 5-yr running mean TC genesis frequency in July–October during 1979–2020. Purple vectors in (a) and dots denote the anomalies that are significant at the 90% confidence level. Only the positive values of 850-hPa absolute vorticity in the main genesis region are shown in (c).

advection $-(\mathbf{V}\cdot\nabla q)'$ is the main factor leading to the negative relative humidity anomalies. Thus, we first divided it into zonal and meridional moisture advection terms, and then found that the negative anomalies of $-(\mathbf{V}\cdot\nabla q)'$ are dominated by the meridional moisture advection $-[v(\partial q/\partial y)]'$. We further decompose it into four terms:

$$-\left(v\frac{\partial q}{\partial y}\right)' = -\left(\overline{v}\frac{\partial \overline{q}}{\partial y}\right)' - \left(\overline{v}\frac{\partial q'}{\partial y}\right)' - \left(v'\frac{\partial \overline{q}}{\partial y}\right)' - \left(v'\frac{\partial q'}{\partial y}\right)'.$$

The overbar denotes the climatological mean, and the prime denotes the anomaly. The term $-[\overline{v}(\partial\overline{q}/\partial y)]'$ represents the anomaly of the mean meridional wind and the mean meridional

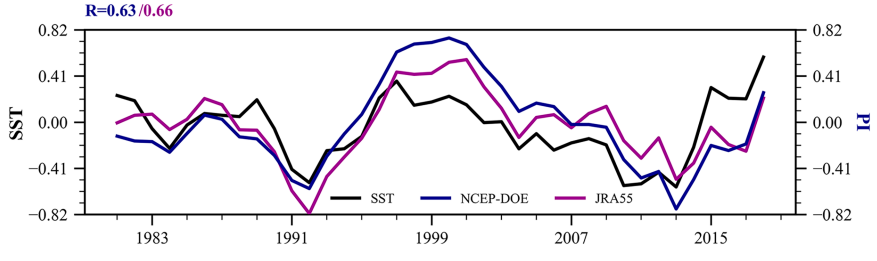

FIG. 7. Time series of 5-yr running mean of SST (black line) and PI over the main genesis region (7.5°–30°N, 110°–170°E) in July–October during 1979–2020 derived from NCEP–DOE (blue line) and JRA-55 reanalysis (purple line). Their correlation coefficients R between SST are shown on the top left of the panel.

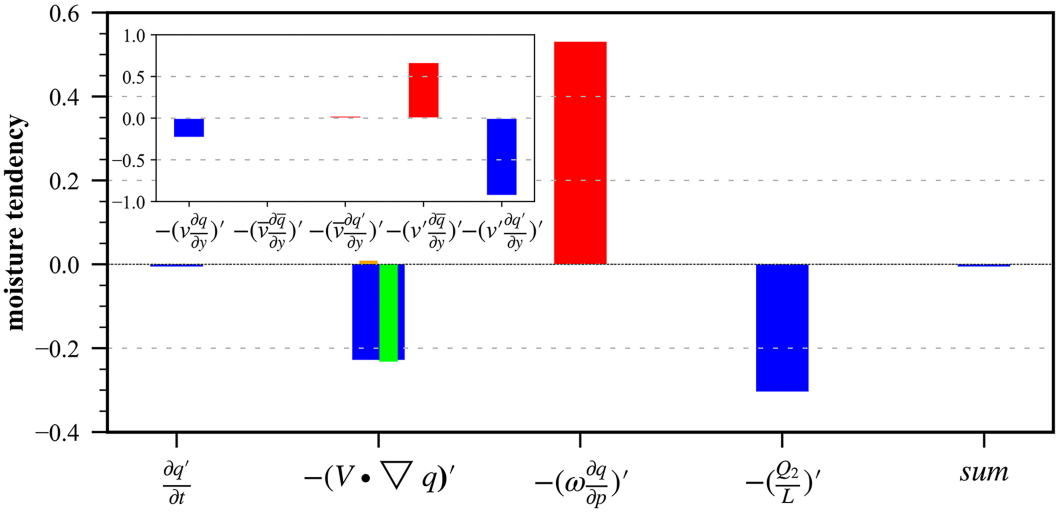

FIG. 8. The 600-hPa moisture budget terms over the main genesis region (7.5°–30°N, 110°–170°E) derived from NCEP–DOE reanalysis. From left to right, the observed specific humidity tendency, horizontal moisture advection, vertical moisture advection, latent heating, and the sum of these budget terms are shown. The orange bar and green bar inside the blue bar denote the contributions of zonal advection and meridional advection, respectively. The contributions of individual terms to the meridional advection are shown in the inset at the top left.

gradient of specific humidity, $-[\overline{v}(\partial q'/\partial y)]'$ indicates the anomalous mean meridional wind and the anomalous meridional gradient of specific humidity, $-[v'(\partial \overline{q}/\partial y)]'$ is the anomaly of the anomalous meridional wind and the mean meridional gradient of specific humidity, and $-[v'(\partial q'/\partial y)]'$ denotes the nonlinear effects between the anomalous meridional wind and the anomalous meridional gradient of specific humidity. It is found that that the nonlinear effects between the anomalous northerly wind and the anomalous meridional gradient of specific humidity $\{-[v'(\partial q'/\partial y)]'\}$ are main contributor to the negative humidity anomalies (Fig. 8).

Thus, the negative SST, MPI, and relative humidity anomalies in the main genesis region are coupled to the enhanced ascending motion and cyclonic vorticity but weakened vertical wind shear therein through the anomalous cyclonic circulation, eventually leading to the opposite effects of the dynamical parameters (enhanced upward motion and cyclonic vorticity, and reduced vertical wind shear) and the thermodynamic parameter (negative MPI and relative humidity) on TC genesis in the WNP. Since the thresholds of thermodynamic parameters for TC genesis generally are satisfied in the warm pool region of the WNP, changes in dynamical parameters play more important roles than the thermodynamic ones in TC formation over the WNP (McBride and Zehr 1981; Lee 1989a,b; Fu et al. 2012). Therefore, the DGPI, integrating the effects of large-scale dynamical parameters, shows positive skill, while the ENGPI, which is generally dominated by the thermodynamic parameters, shows negative skill in depicting the decadal variation of TC genesis in the WNP.

5. Summary and discussion

While both the DGPI and ENGPI possess comparable skills in depicting the climatological feature of TC genesis in the WNP, here we find that the ENGPI and DGPI show opposite skills in depicting the decadal variation of TC genesis over the WNP. Particularly, ENGPI shows an opposite decadal variation to the WNP TC genesis, yielding a significant negative correlation of −0.61. The DGPI can reasonably reproduce the decadal variation of the WNP TC genesis with a significant correlation of 0.66 during 1979–2020. The opposite skill of the two indices stems from the opposite effects of dynamic and thermodynamic parameters on TC genesis that are linked to an anomalous cyclonic circulation controlling the decadal variation of TC genesis in the WNP. On the one hand, the cyclonic circulation results in anomalous ascending motion, cyclonic vorticity, and weakened vertical shear, leading to a favorable dynamical environment for TC genesis and positive DGPI anomalies. On the other hand, the tropical westerly and subtropical northerly anomalies associated with the cyclonic circulation tend to decrease SST (MPI) and dry the midtroposphere, respectively, which collectively contribute to the unfavorable thermodynamic environment and thus negative ENGPI anomalies. Therefore, the negative SST, MPI, and relative humidity anomalies in the main genesis region are coupled to the enhanced ascending motion and cyclonic vorticity and weakened vertical wind shear therein, eventually leading to the opposite effects of dynamical parameters and the thermodynamic parameters on TC genesis in the WNP. Since the threshold of thermodynamic parameters for TC formation generally is satisfied in the warm pool region, dynamical parameters play a more important role than the thermodynamic ones in TC formation in the WNP. Therefore, the DGPI, integrating the effects of dynamic parameters, shows positive skill, while the ENGPI, which is generally dominated by the thermodynamic parameters, shows negative skill in depicting the decadal variation of TC genesis in the WNP.

One may question the skills of other variants of ENGPI in depicting decadal variability of the WNP TC genesis. Here we find that the two variants of ENGPI proposed by Murakami and Wang (2010) and Emanuel (2010) generally show low skill in representing decadal change in the WNP TC genesis. For instance, the revised ENGPI by Murakami and Wang (2010) including the vertical motion term also shows a similar evolution with original ENGPI, which is almost opposite to that in TC genesis. Further examination suggests that the negative contribution of potential intensity term can overwhelm the positive contribution of midlevel vertical motion term, eventually leading to the significantly negative correlation between TC genesis and the revised ENGPI by Murakami and Wang (2010). The results highlight that dynamical large-scale parameters play an important role in the decadal variation of TC genesis over the WNP (Shan and Yu 2020; Dai et al. 2022), while the effects of thermodynamical parameters may be secondary and somewhat misleading if it is considered. Moreover, the superior skill of DGPI in presenting the decadal variability of the WNP TC genesis provides us with a powerful tool to investigate climate variability of TC genesis in the current and future climates.

Acknowledgments. This study was jointly supported by the National Natural Science Foundation of China (Grants 42088101 and 42075031). It is the Earth System Modeling Center publication 408 at Nanjing University of Information Science and Technology. We acknowledge the High-Performance Computer Center of Nanjing University of Information Science and Technology for their support for this work.

Data availability statement. The International Best Track Archive for Climate Stewardship version 4 data were downloaded at https://www.ncei.noaa.gov/products/international-best-track-archive?name=ib-v4-access, NCEP–DOE reanalysis was obtained from https://psl.noaa.gov/data/gridded/data.ncep.reanalysis2.html, JRA-55 reanalysis was obtained from https://rda.ucar.edu/datasets/ds628.1, and SST was downloaded at https://psl.noaa.gov/data/gridded/data.noaa.ersst.v5.html.

REFERENCES

Bister, M., and K. A. Emanuel, 1998: Dissipative heating and hurricane intensity. *Meteor. Atmos. Phys.*, **65**, 233–240, https://doi.org/10.1007/BF01030791.

Bjerknes, J., 1969: Atmospheric teleconnections from the equatorial Pacific. *Mon. Wea. Rev.*, **97**, 163–172, https://doi.org/10.1175/1520-0493(1969)097<0163:ATFTEP>2.3.CO;2.

Camargo, S. J., K. A. Emanuel, and A. H. Sobel, 2007: Use of a genesis potential index to diagnose ENSO effects on tropical cyclone genesis. *J. Climate*, **20**, 4819–4834, https://doi.org/10.1175/JCLI4282.1.

——, M. C. Wheeler, and A. H. Sobel, 2009: Diagnosis of the MJO modulation of tropical cyclogenesis using an empirical index. *J. Atmos. Sci.*, **66**, 3061–3074, https://doi.org/10.1175/2009JAS3101.1.

——, M. K. Tippett, A. H. Sobel, G. A. Vecchi, and M. Zhao, 2014: Testing the performance of tropical cyclone genesis indices in future climates using the HiRAM model. *J. Climate*, **27**, 9171–9196, https://doi.org/10.1175/JCLI-D-13-00505.1.

Dai, Y., B. Wang, N. Wei, J. Song, and Y. Duan, 2022: How has the North Pacific Gyre Oscillation affected peak season tropical cyclone genesis over the western North Pacific from 1965 to 2020? *Environ. Res. Lett.*, **17**, 104016, https://doi.org/10.1088/1748-9326/ac89a1.

Davis, R. E., 1976: Predictability of sea surface temperature and sea level pressure anomalies over the North Pacific Ocean. *J. Phys. Oceanogr.*, **6**, 249–266, https://doi.org/10.1175/1520-0485(1976)006<0249:POSSTA>2.0.CO;2.

DeMaria, M., and J. Kaplan, 1994: Sea surface temperature and the maximum intensity of Atlantic tropical cyclones. *J. Climate*, **7**, 1324–1334, https://doi.org/10.1175/1520-0442(1994)007<1324:SSTATM>2.0.CO;2.

Emanuel, K. A., 1987: The dependence of hurricane intensity on climate. *Nature*, **326**, 483–485, https://doi.org/10.1038/326483a0.

——, 1999: Thermodynamic control of hurricane intensity. *Nature*, **401**, 665–669, https://doi.org/10.1038/44326.

——, 2010: Tropical cyclone activity downscaled from NOAA-CIRES reanalysis, 1908–1958. *J. Adv. Model. Earth Syst.*, **2** (1), https://doi.org/10.3894/JAMES.2010.2.1.

——, 2021: Response of global tropical cyclone activity to increasing CO_2: Results from downscaling CMIP6 models. *J. Climate*, **34**, 57–70, https://doi.org/10.1175/JCLI-D-20-0367.1.

——, and D. S. Nolan, 2004: Tropical cyclone activity and the global climate system. *26th Conf. on Hurricanes and Tropical Meteorology*, Miami, FL, Amer. Meteor. Soc., 10A.2, https://ams.confex.com/ams/26HURR/techprogram/paper_75463.htm.

Fu, B., M. S. Peng, T. Li, and D. E. Stevens, 2012: Developing versus nondeveloping disturbances for tropical cyclone formation. Part II: Western North Pacific. *Mon. Wea. Rev.*, **140**, 1067–1080, https://doi.org/10.1175/2011MWR3618.1.

Gray, W. M., 1968: Global view of the origin of tropical disturbances and storms. *Mon. Wea. Rev.*, **96**, 669–700, https://doi.org/10.1175/1520-0493(1968)096<0669:GVOTOO>2.0.CO;2.

——, 1979: Hurricanes: Their formation, structure and likely role in the tropical circulation. *Meteorology over Tropical Oceans*, D. B. Shaw, Ed., Royal Meteorological Society, 155–218.

Holland, G., and C. L. Bruyère, 2013: Recent intense hurricane response to global climate change. *Climate Dyn.*, **42**, 617–627, https://doi.org/10.1007/s00382-013-1713-0.

Hu, C., C. Zhang, S. Yang, D. Chen, and S. He, 2018: Perspective on the northwestward shift of autumn tropical cyclogenesis locations over the western North Pacific from shifting ENSO. *Climate Dyn.*, **51**, 2455–2465, https://doi.org/10.1007/s00382-017-4022-1.

Huang, B., and Coauthors, 2017: Extended Reconstructed Sea Surface Temperature, version 5 (ERSSTv5): Upgrades, validations, and intercomparisons. *J. Climate*, **30**, 8179–8205, https://doi.org/10.1175/JCLI-D-16-0836.1.

Kanamitsu, M., W. Ebisuzaki, J. Woollen, S.-K. Yang, J. J. Hnilo, M. Fiorino, and G. L. Potter, 2002: NCEP–DOE AMIP-II Reanalysis (R-2). *Bull. Amer. Meteor. Soc.*, **83**, 1631–1644, https://doi.org/10.1175/BAMS-83-11-1631.

Knapp, K. R., M. C. Kruk, D. H. Levinson, H. J. Diamond, and C. J. Neumann, 2010: The International Best Track Archive for Climate Stewardship (IBTrACS). *Bull. Amer. Meteor. Soc.*, **91**, 363–376, https://doi.org/10.1175/2009BAMS2755.1.

Knutson, T., and Coauthors, 2020: Tropical cyclones and climate change assessment. Part II: Projected response to anthropogenic warming. *Bull. Amer. Meteor. Soc.*, **101**, E303–E322, https://doi.org/10.1175/BAMS-D-18-0194.1.

Kobayashi, S., and Coauthors, 2015: The JRA-55 reanalysis: General specifications and basic characteristics. *J. Meteor. Soc. Japan*, **93**, 5–48, https://doi.org/10.2151/jmsj.2015-001.

Lee, C. S., 1989a: Observational analysis of tropical cyclogenesis in the western North Pacific. Part I: Structural evolution of cloud clusters. *J. Atmos. Sci.*, **46**, 2580–2598, https://doi.org/10.1175/1520-0469(1989)046<2580:OAOTCI>2.0.CO;2.

——, 1989b: Observational analysis of tropical cyclogenesis in the western North Pacific. Part II: Budget analysis. *J. Atmos. Sci.*, **46**, 2599–2616, https://doi.org/10.1175/1520-0469(1989)046<2599:OAOTCI>2.0.CO;2.

Liu, K. S., and J. C. L. Chan, 2013: Inactive period of western North Pacific tropical cyclone activity in 1998–2011. *J. Climate*, **26**, 2614–2630, https://doi.org/10.1175/JCLI-D-12-00053.1.

McBride, J. L., and R. Zehr, 1981: Observational analysis of tropical cyclone formation. Part II: Comparison of non-developing versus developing systems. *J. Atmos. Sci.*, **38**, 1132–1151, https://doi.org/10.1175/1520-0469(1981)038<1132:OAOTCF>2.0.CO;2.

Menkes, C. E., M. Lengaigne, P. Marchesiello, N. C. Jourdain, E. M. Vincent, J. Lefèvre, F. Chauvin, and J.-F. Royer, 2011: Comparison of tropical cyclogenesis indices on seasonal to interannual timescales. *Climate Dyn.*, **38**, 301–321, https://doi.org/10.1007/s00382-011-1126-x.

Moon, J. Y., B. Wang, S.-S. Lee, and K.-J. Ha, 2018: An intraseasonal genesis potential index for tropical cyclones during Northern Hemisphere summer. *J. Climate*, **31**, 9055–9071, https://doi.org/10.1175/JCLI-D-18-0515.1.

Murakami, H., and B. Wang, 2010: Future change of North Atlantic tropical cyclone tracks: Projection by a 20-km-mesh global atmospheric model. *J. Climate*, **23**, 2699–2721, https://doi.org/10.1175/2010JCLI3338.1.

——, and ——, 2022: Patterns and frequency of projected future tropical cyclone genesis are governed by dynamic effects. *Commun. Earth Environ.*, **3**, 77, https://doi.org/10.1038/s43247-022-00410-z.

Reid, G. C., and K. S. Gage, 1981: On the annual variation in height of the tropical tropopause. *J. Atmos. Sci.*, **38**, 1928–1938, https://doi.org/10.1175/1520-0469(1981)038<1928:OTAVIH>2.0.CO;2.

Roberts, M. J., and Coauthors, 2020: Projected future changes in tropical cyclones using the CMIP6 HighResMIP multimodel ensemble. *Geophys. Res. Lett.*, **47**, e2020GL088662, https://doi.org/10.1029/2020GL088662.

Shan, K., and X. Yu, 2020: Interdecadal variability of tropical cyclone genesis frequency in western North Pacific and South Pacific Ocean basins. *Environ. Res. Lett.*, **15**, 064030, https://doi.org/10.1088/1748-9326/ab8093.

Tippett, M. K., S. J. Camargo, and A. H. Sobel, 2011: A Poisson regression index for tropical cyclone genesis and the role of large-scale vorticity in genesis. *J. Climate*, **24**, 2335–2357, https://doi.org/10.1175/2010JCLI3811.1.

Wang, B., and LinHo, 2002: Rainy season of the Asian-Pacific summer monsoon. *J. Climate*, **15**, 386–398, https://doi.org/10.1175/1520-0442(2002)015<0386:RSOTAP>2.0.CO;2.

——, and J.-Y. Moon, 2017: An anomalous genesis potential index for MJO modulation of tropical cyclones. *J. Climate*, **30**, 4021–4035, https://doi.org/10.1175/JCLI-D-16-0749.1.

——, and H. Murakami, 2020: Dynamic genesis potential index for diagnosing present-day and future global tropical cyclone genesis. *Environ. Res. Lett.*, **15**, 114008, https://doi.org/10.1088/1748-9326/abbb01.

——, K. Wu, L. Wu, H. Zhao, and J. Cao, 2021: What caused the unprecedented absence of western North Pacific tropical cyclones in July 2020? *Geophys. Res. Lett.*, **48**, e2020GL092282, https://doi.org/10.1029/2020GL092282.

Wang, C., and L. Wu, 2016: Interannual shift of the tropical upper-tropospheric trough and its influence on tropical cyclone formation over the western North Pacific. *J. Climate*, **29**, 4203–4211, https://doi.org/10.1175/JCLI-D-15-0653.1.

——, and B. Wang, 2019: Tropical cyclone predictability shaped by western Pacific subtropical high: Integration of trans-basin sea surface temperature effects. *Climate Dyn.*, **53**, 2697–2714, https://doi.org/10.1007/s00382-019-04651-1.

——, and ——, 2021: Impacts of the South Asian high on tropical cyclone genesis in the South China Sea. *Climate Dyn.*, **56**, 2279–2288, https://doi.org/10.1007/s00382-020-05586-8.

——, ——, L. Wu, and J.-J. Luo, 2022: A seesaw variability in tropical cyclone genesis between the western North Pacific and the North Atlantic shaped by Atlantic multidecadal variability. *J. Climate*, **35**, 2479–2489, https://doi.org/10.1175/JCLI-D-21-0529.1.

Weng, J., L. Wang, J. Luo, B. Chen, X. Peng, and Q. Gan, 2022: A contrast of the monsoon–tropical cyclone relationship between the western and eastern North Pacific. *Atmosphere*, **13**, 1465, https://doi.org/10.3390/atmos13091465.

Wilks, D. S., 2006: *Statistical Methods in the Atmospheric Sciences*. Academic Press, 676 pp.

Wu, L., C. Wang, and B. Wang, 2015: Westward shift of western North Pacific tropical cyclogenesis. *Geophys. Res. Lett.*, **42**, 1537–1542, https://doi.org/10.1002/2015GL063450.

Yanai, M., S. Esbensen, and J.-H. Chu, 1973: Determination of bulk properties of tropical cloud clusters from large-scale heat and moisture budgets. *J. Atmos. Sci.*, **30**, 611–627, https://doi.org/10.1175/1520-0469(1973)030<0611:DOBPOT>2.0.CO;2.

Zhang, M., L. Zhou, D. Chen, and C. Wang, 2016: A genesis potential index for western North Pacific tropical cyclones by using oceanic parameters. *J. Geophys. Res. Oceans*, **121**, 7176–7191, https://doi.org/10.1002/2016JC011851.

Zhao, H., X. Jiang, and L. Wu, 2015: Modulation of northwest Pacific tropical cyclone genesis by the intraseasonal variability. *J. Meteor. Soc. Japan*, **93**, 81–97, https://doi.org/10.2151/jmsj.2015-006.